

# Chapter 5

## The Meridional Structure of the Atmosphere

In previous chapters we considered those processes that play a role in setting the vertical distribution of atmospheric properties. Here we discuss how these properties vary horizontally, on the global scale. We shall see that geometrical effects play a major role in setting the observed horizontal distribution. The spherical Earth intercepts an essentially parallel beam of solar radiation and so the incoming flux *per unit surface area* is greater at the equator than at the pole. An obvious and important consequence is that the atmosphere in the equatorial belt is warmer (and hence moister) than the atmosphere over the polar caps. As we will discuss in this and subsequent chapters, these horizontal temperature gradients induce horizontal pressure gradients and hence motions, as sketched in Fig.5.1. The resulting atmospheric wind patterns (along with ocean currents) act to transport heat from the warm tropics to the cool high latitudes, thereby playing a major role in climate.

In this Chapter, then, we will describe the observed climatology<sup>1</sup> of atmospheric temperature, pressure, humidity and wind.

---

<sup>1</sup>Here "climatology" implies some appropriate long-term average, such as the annual mean, or seasonal mean, averaged over many years. In many of the figures shown here, the data are also averaged over longitude.

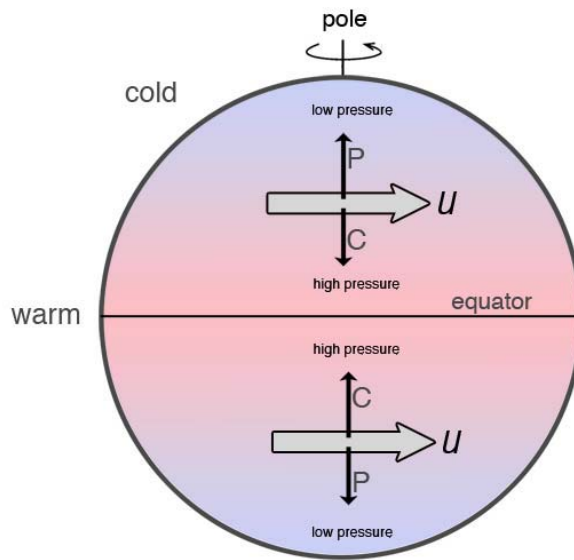


Figure 5.1: The atmosphere is warmer in the equatorial belt than over the polar caps. These horizontal temperature gradients induce, by hydrostatic balance, a horizontal pressure gradients force ‘P’ that drive rings of air poleward. Conservation of angular momentum induces the rings to accelerate eastwards until Coriolis forces acting on them, ‘C’, are sufficient to balance the pressure gradient force ‘P’, as discussed in Chapters 6 and 7.

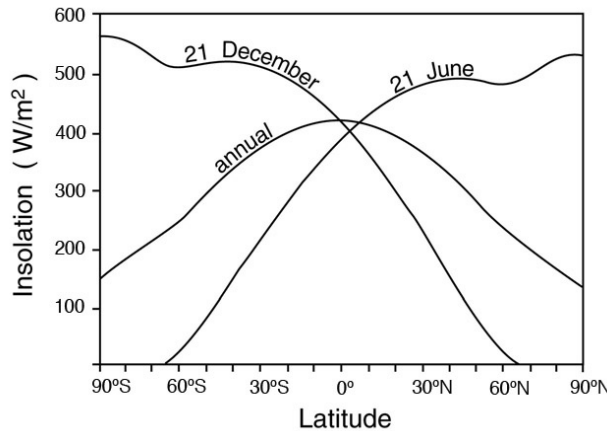


Figure 5.2: Distribution of annual mean and solstice (see Fig.5.4) incoming solar radiation. The slight dip in the distribution at, for example, the winter solstice (December 21st) in the southern hemisphere, corresponds to the edge of the polar day.

## 5.1 Radiative forcing and Temperature

### 5.1.1 Incoming radiation

#### Annual mean

The latitudinal distribution of incoming solar radiation at the top of the atmosphere in the annual mean and at solstice is shown in Fig.5.2. Its distribution is a consequence of the spherical geometry of the earth and the tilt of the spin axis, depicted in Fig.5.3. If the Earth's axis did not tilt with respect to the orbital plane, the average incident flux would maximize at a value of  $S_{\max} = S_0/\pi = 435 \text{ W m}^{-2}$  at the equator, and fall monotonically to zero at the poles. Because of the tilt, however, the poles do receive solar radiation during the summer half-year, and therefore the annual-mean equator-to-pole difference is reduced, as Fig.5.2 makes clear.

#### Seasonal

The daily averaged radiation received at any point on Earth varies through the year, for two reasons. First, as illustrated in Fig.5.4, the Earth's orbit

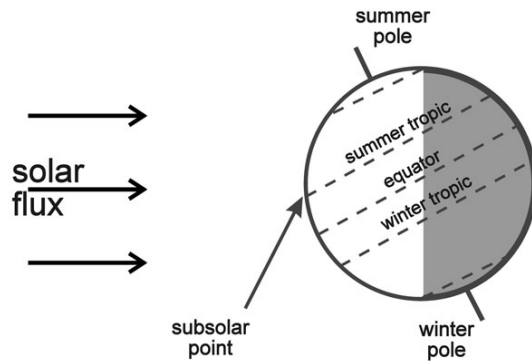


Figure 5.3: At the present time in history, the earth's axis tilts at  $23.5^\circ$  and points towards the North Star. We sketch the incoming solar radiation at summer solstice when the earth is tilted toward the sun.

around the Sun is not circular; the Earth is in fact closest to the Sun — and the solar flux incident at the top of the atmosphere therefore maximizes — just after northern winter solstice. However, the variation of the Earth-Sun distance is less than  $\pm 2\%$ ; while the corresponding variation in solar flux is not negligible, its contribution to the annual variation of the local solar flux per unit area at any given latitude is much less than that arising from the tilt of the rotation axis. At the present time in Earth history, the spin axis tilts from the vertical by  $23.5^\circ$ , the north pole pointing almost toward the North Star. At northern summer solstice, the north pole is tipped in the direction of the Sun, and the northern hemisphere has the longest day of the year. Conversely, at the northern winter solstice the north pole is tipped away from the Sun, and the northern hemisphere has the shortest day. At the equinoxes, daytime and nighttime are of equal length.

At solstice there is no incoming radiation at the winter pole (nor anywhere within “polar night”), but there is sunlight 24 hours a day at the summer pole. It is for this reason that the incoming radiation actually maximizes (slightly) at the summer pole, when averaged over 24 hrs, as shown in Fig.5.2. Nevertheless, the absorbed radiation at the summer pole is low because of the high albedo of snow and ice.

Before going on, we should emphasize that the Earth's tilt and its orbit around the Sun are not constant but change on very long time scales (of order  $10^4 - 10^5$  yr) in what are known as Milankovitch cycles. These changes

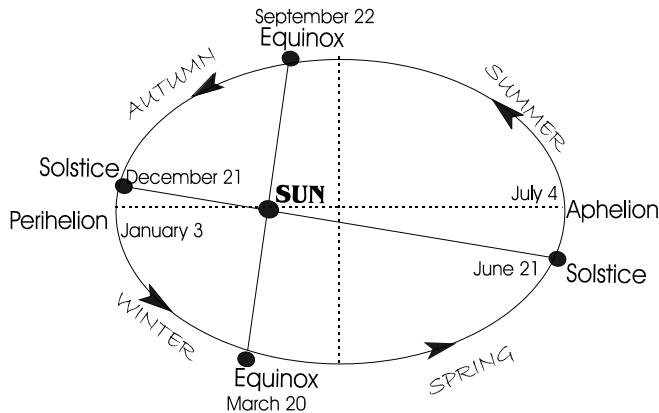


Figure 5.4: Earth describes an elliptical orbit around the Sun, greatly exaggerated in the figure. The longest (shortest) day occurs at the summer (winter) solstice when the earth's spin axis points toward (away from) the sun. The Earth is farthest from (closest to) the Sun at aphelion (perihelion). The seasons are labelled for the Northern hemisphere.

are thought to play a role in climate change on very long timescales and, perhaps, in pacing glacial-interglacial cycles, as will be discussed in Section 12.3.5.

### 5.1.2 Outgoing radiation

The net radiative budget of the Earth-atmosphere system, averaged over the year, is shown in Fig.5.5. The absorbed solar (incoming minus reflected) has a strong maximum in the tropics, where it is about 6 times larger than at the poles. The latitudinal variation of emitted longwave radiation, however, is much less, implying that the actual pole-to-equator temperature difference is smaller than it would be if the atmosphere were in thermodynamic balance at each latitude, column by column. Averaged over the year, there is a net surplus of incoming radiation in the tropics, and a net deficit at high latitudes. Since local energy balance must be satisfied, Fig.5.5 implies that there must be a transport of energy from low to high latitudes to maintain equilibrium (see Q.1 at end of Chapter).

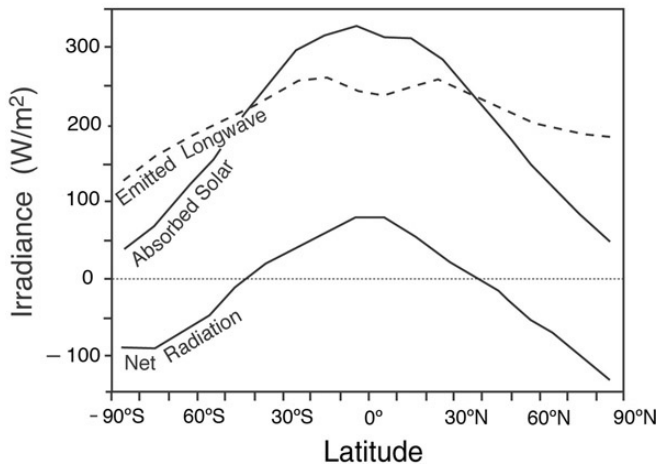


Figure 5.5: Annual mean absorbed solar radiation, emitted longwave radiation and net radiation, the sum of the two. The slight dip in emitted longwave radiation at the equator is due to radiation from the (cold) tops of deep convecting clouds, as can be seen in Fig.4.26.

### 5.1.3 The energy balance of the atmosphere

The required transport is quantified and plotted in Fig.5.6 based on satellite measurements of incoming and outgoing solar and terrestrial radiation at the top of the atmosphere (see Section 11.5). In each hemisphere, the implied flux of energy is around  $6 \times 10^{15} W = 6 PW$ .<sup>2</sup> As will be discussed in the following chapters (particularly Chapters 8 and 11), the transport is achieved by fluid motions, especially in the atmosphere, but with the ocean also making a significant contribution.

### 5.1.4 Meridional structure of temperature

#### Troposphere

The observed structure of annual-mean temperature  $\bar{T}$  (where the overbar implies zonal-average<sup>3</sup>) and potential temperature  $\bar{\theta}$  in the troposphere and

---

<sup>2</sup>1 PW (petawatt) =  $10^{15} W$ .

<sup>3</sup>The zonal average of a quantity  $X$  is conventionally written  $\overline{X}$  (with an overbar) where:

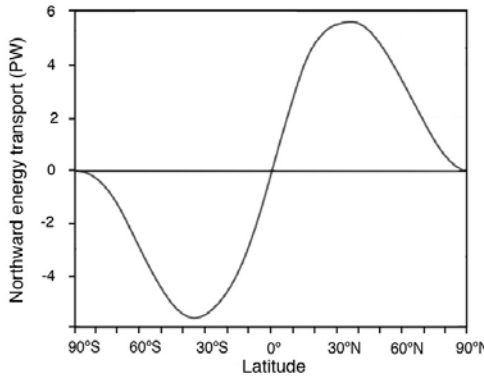


Figure 5.6: The northward energy transport deduced by top of the atmosphere measurements of incoming and outgoing solar and terrestrial radiation from the ERBE satellite. The units are in  $PW = 10^{15} \text{ W}$  — see Trenberth and Caron (2001). This curve is deduced by integrating the ‘net radiation’ plotted in Fig.5.4 meridionally. See Chapter 11 for a more detailed discussion.

lower stratosphere are shown in Figs.5.7 and 5.8 respectively. Temperature decreases upward and (generally) poleward in the troposphere. The annual average surface temperature is below  $0^\circ\text{C}$  polewards of about  $60^\circ$  latitude, and reaches a maximum of  $27^\circ\text{C}$  just north of the equator. The annual-mean pole-to-equator temperature difference over the troposphere is typically  $40^\circ\text{C}$ .

As can be seen in Fig.5.8, surfaces of constant potential temperature — often referred to as isentropic surfaces (constant  $\theta$  implies constant entropy; see Q.5 of Chapter 4) — slope upwards towards the pole in the troposphere. Moreover  $\bar{\theta}$  (unlike  $\bar{T}$ ) always increases with height, reflecting the stability of the atmosphere to dry processes discussed in Section 4.3.2. The closely spaced contours aloft mark the stratosphere, the widely spaced contours below mark the troposphere. The transition between the two, the tropopause, is higher in the tropics than over the pole.

---


$$\bar{X}(\varphi, z) = \frac{1}{2\pi} \int_0^{2\pi} X(\lambda, \varphi, z) d\lambda$$

$(\lambda, \varphi)$  being (longitude, latitude).

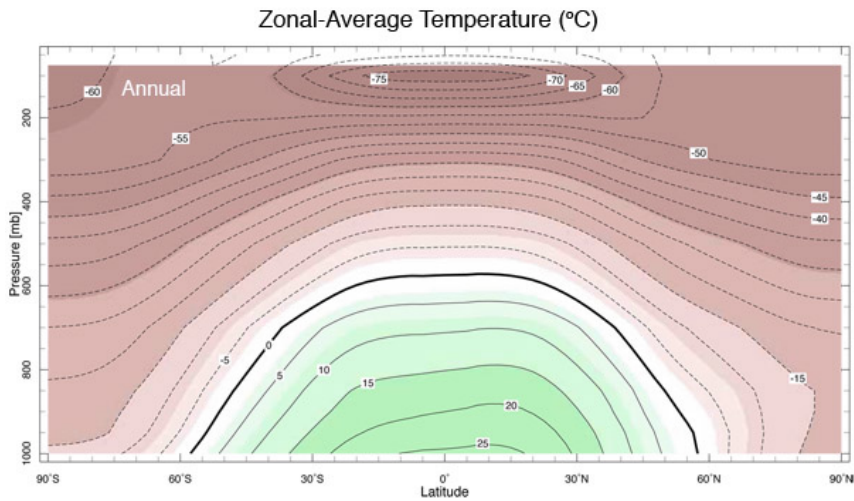


Figure 5.7: The zonally averaged annual mean temperature in °C.

Fig.5.9 shows the annual-mean equivalent potential temperature,  $\theta_e$ , defined by Eq.(4.30), and vividly displays the effects of vigorous convection in the tropics which remove vertical gradients of  $\theta_e$ . This should be contrasted with the large vertical gradients of dry potential temperature,  $\theta$ , seen in Fig.5.8.

### Stratosphere

The zonally averaged temperature is again shown in Fig.5.10 (plotted here against height, rather than pressure, to emphasize upper altitudes) for solstice conditions. The features of the vertical temperature structure discussed in Chapter 3.1 are even clearer in Fig.5.10: the temperature minima at the tropopause (at a height of 10 – 16 km) and mesopause (near 80 km), and the maximum at the stratopause (near 50 km). Note the latitudinal variation of these features, especially the variation of the tropopause, which is high and cold in the tropics, and much lower and warmer in high latitudes. In fact, there is something like a discontinuity of the tropopause in the subtropics (the so-called “tropopause gap”) which, as we will see in Chapter 8, is associated with the presence of strong winds — the ‘jet stream’. Air moving between the troposphere and stratosphere in a vertical direction (upward in

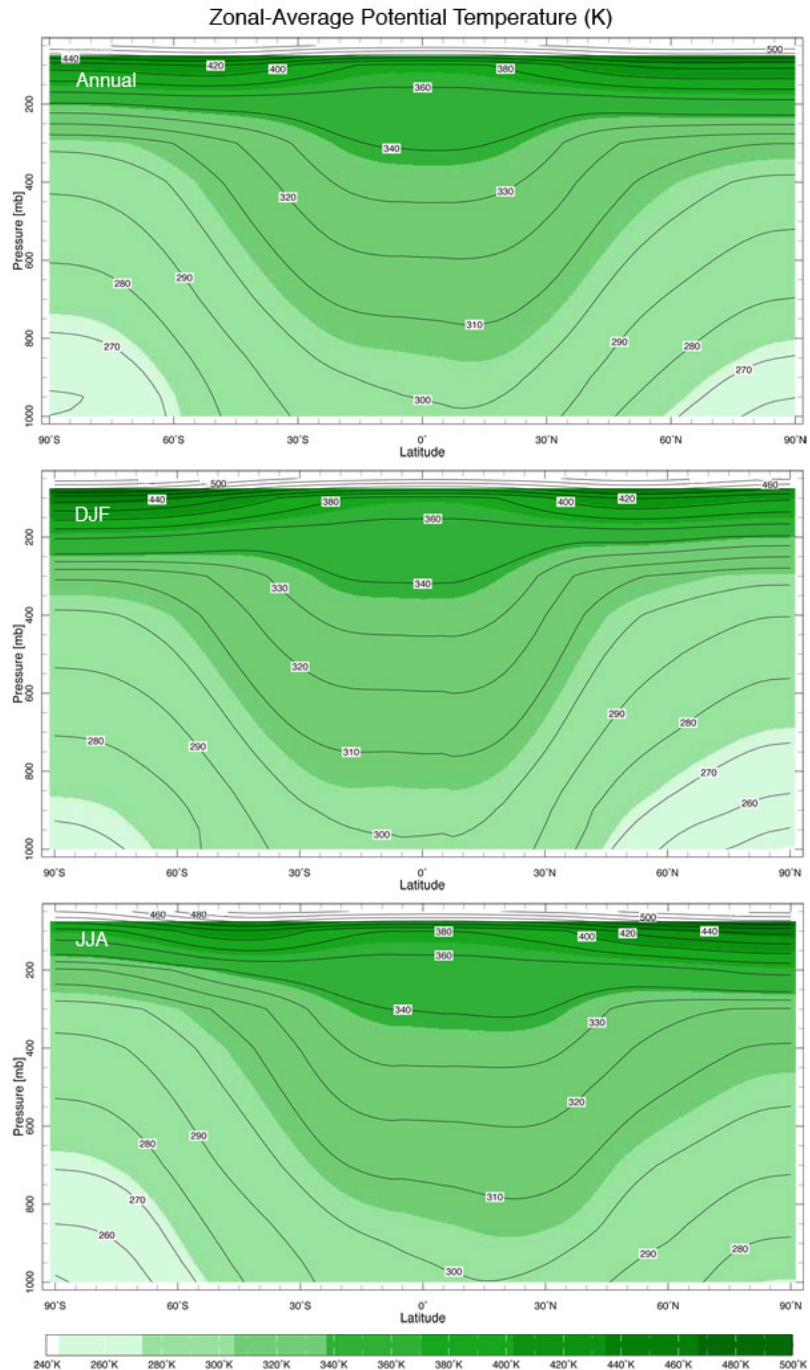


Figure 5.8: The zonally averaged potential temperature in (top) the annual mean, and averaged over (middle) December, January and February (DJF) and (bottom) June, July and August (JJA).

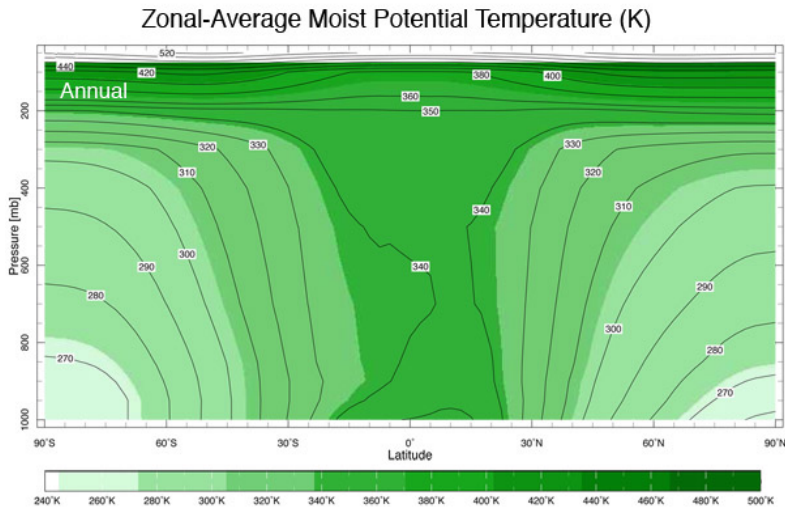


Figure 5.9: The zonal average, annual-mean equivalent potential temperature,  $\theta_e$ , Eq.(4.30).

the tropics, downward in the extratropics) does so very slowly, so that it has time to adjust its potential temperature to ambient values in response to weak diabatic processes. However, air can be exchanged more rapidly across the tropopause gap since it can do so adiabatically by moving almost horizontally along isentropic surfaces between the tropical upper troposphere and the extra-tropical lower stratosphere.

The latitudinal temperature variation of the stratosphere is consistent with the incoming radiation budget: its temperature is greatest at the summer pole, where the averaged incoming radiation is most intense. However, in the troposphere the pole remains far colder than the tropics, even in summer. The polar regions, after a long cold winter, remain covered in highly reflective ice and snow (which do not have time to melt over the summer) and so have a high albedo (typically around 60%, compared to the global average of about 30%; *cf.* Fig. 2.4 and Table 2.2). Thus, the solar radiation absorbed at the surface is substantially lower at the poles than in the tropics, even in summer.

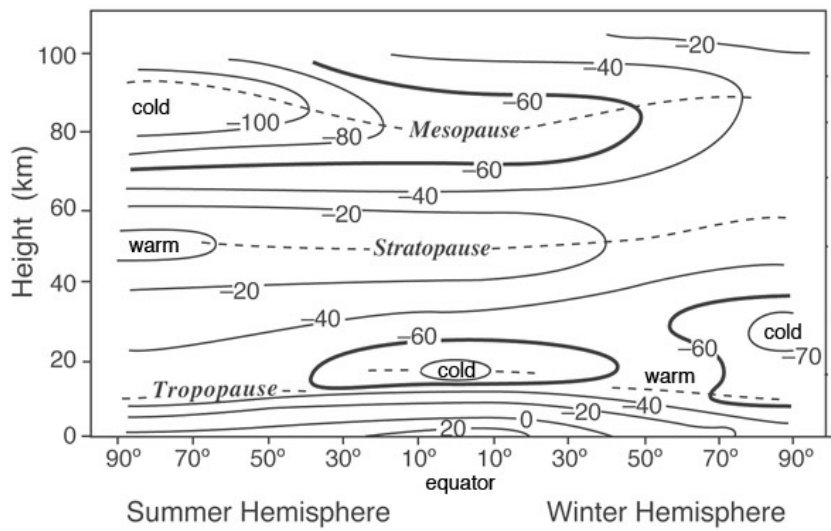


Figure 5.10: The observed, longitudinally-averaged temperature distribution ( $T$ ) at northern summer solstice from the surface to a height of 100 km (after Houghton, 1986). Altitudes at which the vertical  $T$  gradient vanishes are marked by the dotted lines and correspond to the demarcations shown on the  $T(z)$  profile in Fig.3.1. The  $-60^{\circ}\text{C}$  isopleth is thick. Note the vertical scale is in km compared to Fig.5.7 which is in pressure. To convert between them, use Eq.(3.8).

## 5.2 Pressure and geopotential height

We have seen that it is warmer in the tropics than at higher latitudes. We will now describe how, through hydrostatic balance, this warmth leads to expansion of tropical air columns relative to polar air columns and hence meridional pressure gradients. It is these pressure gradients that induce fluid accelerations and hence winds.

It is customary in meteorology to use pressure, rather than height, as the primary vertical coordinate. Some conceptual reasons will become clear in Chapter 6. Since, in hydrostatic balance, pressure is directly related to the overlying mass burden, pressure is actually a mass coordinate. In observations, it is simpler to measure pressure *in situ* than height, so there are practical advantages also.<sup>4</sup>

With  $p$  as a vertical coordinate, height  $z$  becomes a *dependent variable*, so we now speak of  $z(p)$  — the height of a pressure surface — rather than  $p(z)$ . In principle, this is a trivial change: we can easily take a plot of  $p(z)$ , such as Fig.3.6, and lay it on its side to give us  $z(p)$ . From Eq.(3.5) we may then write:

$$\frac{\partial z}{\partial p} = -\frac{RT}{gp}, \quad (5.1)$$

or, noting that  $p\frac{\partial}{\partial p} = \frac{\partial}{\partial \ln p}$ ,

$$\frac{\partial z}{\partial \ln p} = -\frac{RT}{g} = -H$$

where  $H$  is the vertical scale height, Eq.(3.9). For an isothermal atmosphere (with constant scale height),  $z$  varies as  $\ln p$ , which of course is just another way of saying that  $p$  varies exponentially with  $z$  (see Eqs.3.7 and 3.8). By integrating Eq.(5.1) vertically we see that the height of a given pressure



<sup>4</sup> Evangelista Torricelli (1608-1647) was the first person to create a sustained vacuum. He discovered the principle of the barometer which led to the development of the first instrument to measure pressure.

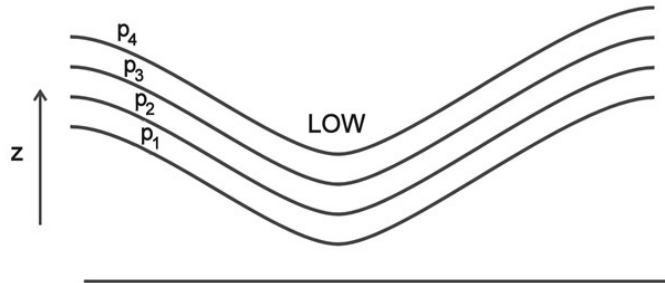


Figure 5.11: The geometry of pressure surfaces (surfaces of constant  $p_1, p_2, p_3, p_4$ , where  $p_1 > p_2 > p_3 > p_4$ ) in the vicinity of a horizontal pressure minimum.

surface is dependent on the average temperature below that surface and the surface pressure,  $p_s$  thus:

$$z(p) = R \int_p^{p_s} \frac{T}{g} \frac{dp}{p} . \quad (5.2)$$

where we have set  $z(p_s) = 0$ . The *geopotential height* of the surface is defined by Eq.(5.2), but with  $g$  replaced by its (constant) surface value. In Chapter 1 we noted that  $g$  varies very little over the depth of the lower atmosphere and so, for most meteorological purposes, the difference between actual height and geopotential height is negligible. In the mesosphere, however, at heights above 100 km, the difference may become significant (see, e.g. Q.6 in Chapter 3).

Note that, as sketched in Fig.5.11, low height of a pressure surface corresponds to low pressure on a  $z$  surface.

The height of the 500 mbar surface (January monthly average) is plotted in Fig.5.12. It has an average height of some 5.5 km, as we deduced in Section 3.3, but is higher in the tropics (5.88 km) than over the pole (4.98 km), sloping down from equator to pole by about 900 m.

The zonally averaged geopotential height is plotted in Fig.5.13 as a function of pressure and latitude for mean annual conditions. Note that the difference  $\bar{z}(\varphi, p) - \langle z \rangle(p)$  is plotted where  $\langle z \rangle(p)$  is the horizontal average at pressure level  $p$ . Except near the surface, pressure surfaces are generally high in the tropics and low at high latitudes, especially in winter. Since surface pressure does not vary much (a few tens of mbar at most), the height of a

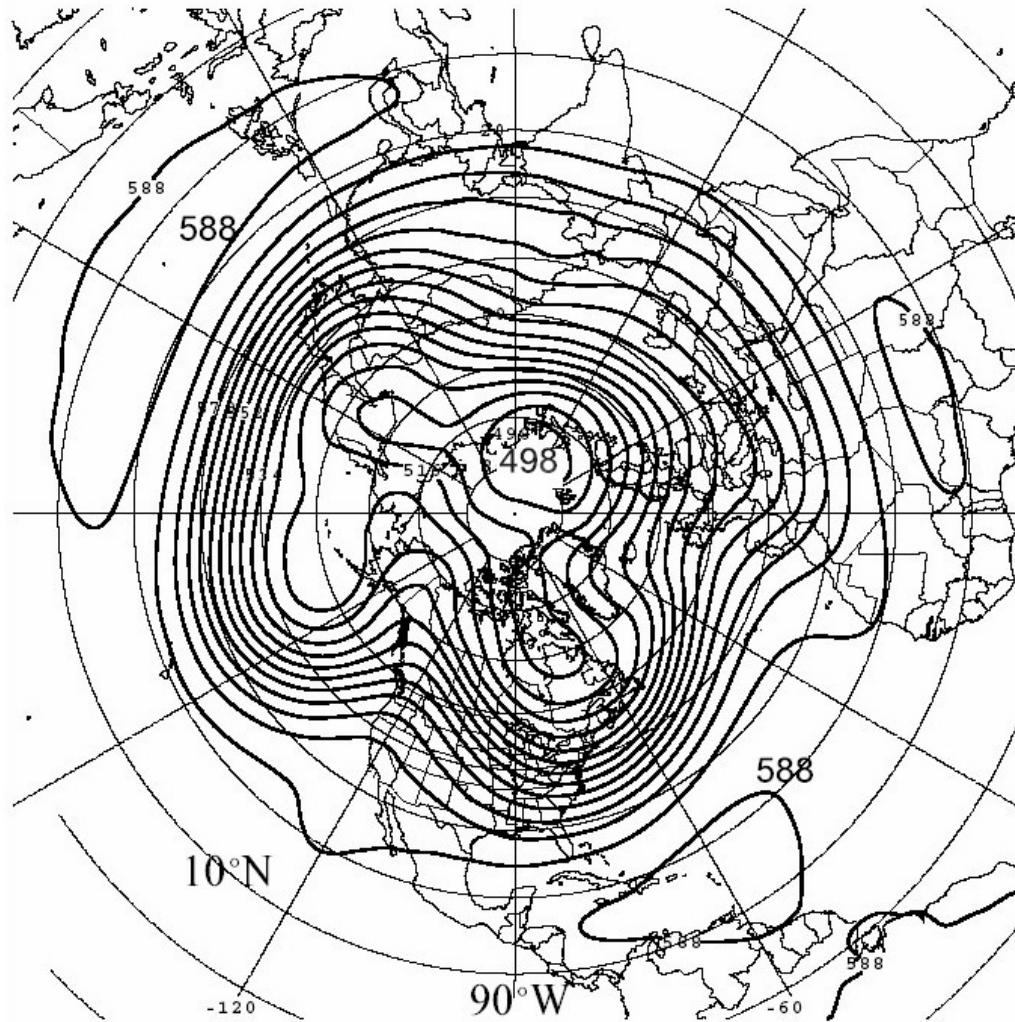


Figure 5.12: The mean height of the 500 mbar surface in January, 2003 (monthly-mean). The contour interval is 6 decameters  $\equiv$  60 m. The surface is 5.88 km high in the tropics and 4.98 km high over the pole. Latitude circles are marked every 10°, longitude every 30°.

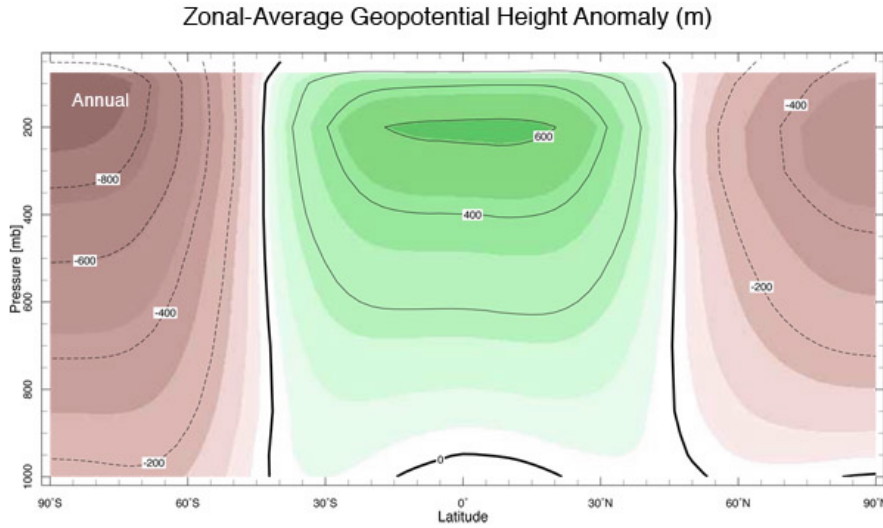


Figure 5.13: Zonal-mean geopotential height ( m) for annual mean conditions. Values are departures from a horizontally uniform reference profile.

given pressure surface is proportional to the mean temperature between that pressure surface and the ground. So, where temperatures are cold (warm), air columns contract (expand) and geopotential heights are low (high).

We can estimate the expected tilt of a pressure surface as follows. For an atmosphere in which  $T$  varies in the horizontal but is vertically isothermal, the difference in the height of an isobaric surface,  $p$ , between warm and cold latitudes,  $\Delta z_{\text{cold}}^{\text{warm}}$  is, using Eq.(3.8):

$$\Delta z_{\text{cold}}^{\text{warm}} = \frac{R\Delta T_{\text{cold}}^{\text{warm}}}{g} \ln \left( \frac{p_s}{p} \right) \quad (5.3)$$

where  $p_s$  is the pressure at the surface. If  $\Delta T_{\text{cold}}^{\text{warm}} = 40^\circ\text{C}$  in the climatology, inserting numbers in to the above, we find that the 500 mbar surface drops by  $\Delta z_{\text{cold}}^{\text{warm}} = 811 \text{ m}$ , as is evident in Figs. 5.12 and 5.13.

Finally, it is useful to define the *thickness* of an atmospheric layer, sandwiched between two pressure surfaces such as  $p_1$  and  $p_2$  in Fig.5.14. From Eq.(5.2) we have:

$$z_2 - z_1 = R \int_{p_2}^{p_1} \frac{T}{g} \frac{dp}{p} . \quad (5.4)$$

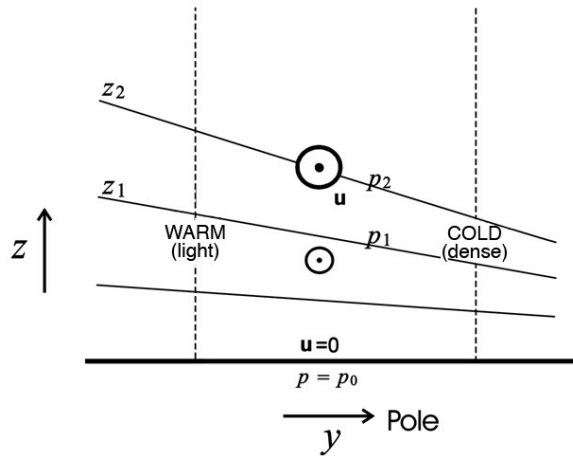


Figure 5.14: Warm columns of air expand, cold columns contract, leading to a tilt of pressure surfaces, a tilt which typically increases with height in the troposphere. In Section 7.3, we will see that the corresponding winds are into the paper, and as marked by  $\odot$  in the figure.

which depends on  $T$  averaged over the layer. Atmospheric layers are ‘thick’ in tropical regions because they are warm and ‘thin’ in polar regions because they are cold, leading to the large-scale slope of pressure surfaces seen in Fig.5.12. Moreover, if tropical columns are warmer than polar columns at all levels, then the tilt of the pressure surfaces must increase with height, as sketched in Fig.5.14 and seen in the observations, Fig.5.13. We will see the importance of this fact when we discuss the distribution of atmospheric winds in Chapter 7.

### 5.3 Moisture

As discussed in Sections 1.3.2 and 4.5, the moisture distribution in the atmosphere is strongly controlled by the temperature distribution: the atmosphere is moist near the surface in the tropics where it is very warm and drier aloft and in polar latitudes where it is cold. As shown in Fig.5.15, the specific humidity, defined in Eq.(4.23), reaches a maximum (of around  $18 \text{ g kg}^{-1}$ ) at the surface near the equator and decreases to much lower values

(around  $1 - 2 \text{ g kg}^{-1}$ ) near the poles. At upper levels there is very little water vapor. This broad pattern can be understood by noting the striking correlation between  $q$  (Fig.5.15) and  $T$  (Fig.5.7). Air colder than  $0^\circ\text{C}$  can hold very little water vapor (see Fig.1.3 and discussions in Section 1.3 and 4.5).

The control by temperature of the specific humidity distribution can be seen more directly by comparing Fig.5.15 with Fig.5.16, which shows  $q_*$ , the specific humidity at saturation given by Eq.(4.24) with  $e_s$  given by Eq.(1.4). We see that  $q$  has the same spatial form as  $q_*$  but never reaches saturation even at the surface. As discussed in Section 4.5,  $U$ , the *relative humidity* defined in Eq.(4.25), is the ratio of  $q$  in Fig.5.15 to  $q_*$  in Fig.5.16. Zonal mean relative humidity, shown in Fig.5.17, is (on average) 70-80% everywhere near the ground. The reason for the decrease of relative humidity with altitude is a little more subtle. Vertical transport of water vapor is effected mostly by convection which (as we have seen) lifts the air to saturation. It may therefore seem odd that even the relative humidity decreases significantly with height through the troposphere. In order to understand this, we need to think about the entire circulation of a convective system, and not just the updraft. Consider Fig.5.18.

The updraft in a convective cloud — the part considered in the parcel stability argument of Section 4.5.2 — is rather narrow. Of course, the air must return and does so in a broad downdraft. Now, within the updraft, the air becomes saturated (whence the cloud) and will frequently produce precipitation: the excess water will rain out. Therefore, even though the air is saturated within the cloud, by the time the air flows out from the top of the cloud, it has lost most of its water (since the cloud top is at much lower temperature than the ground, and hence its saturation specific humidity is very low). As this air descends and warms within the downdraft, it conserves its specific humidity. Since, once it has warmed, the saturation specific humidity at the air temperature has increased, the air becomes very dry, in the sense that its relative humidity is very low. Hence, even though the air is saturated within the updraft, the average (at a fixed height), over the system as a whole, is low. Convection, by lifting air to saturation and thus causing precipitation of the air's water, acts as a drying agent for the atmosphere. This can be vividly seen in the satellite mosaic of the water vapor distribution over the globe between heights of about  $6 - 10 \text{ km}$  is shown in Fig.3 of the Preface. The regions of relatively dry descent (dark regions) on either side of the equatorial moist band (light), mark the latitude

140 CHAPTER 5. THE MERIDIONAL STRUCTURE OF THE ATMOSPHERE

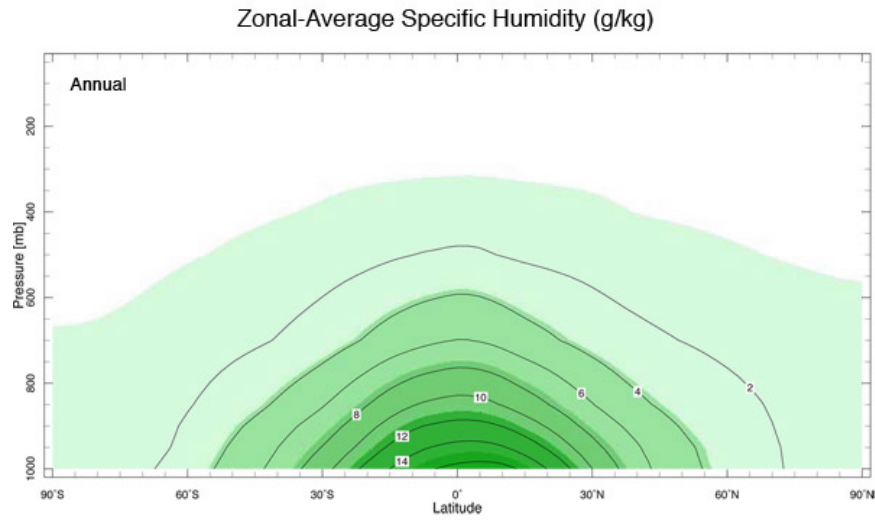


Figure 5.15: Zonally averaged specific humidity  $q$  — Eq.(4.23) in  $\text{g kg}^{-1}$  — under annual mean conditions. Note that almost all the water vapor in the atmosphere is found where  $T > 0^\circ\text{C}$  — see Fig.5.7.

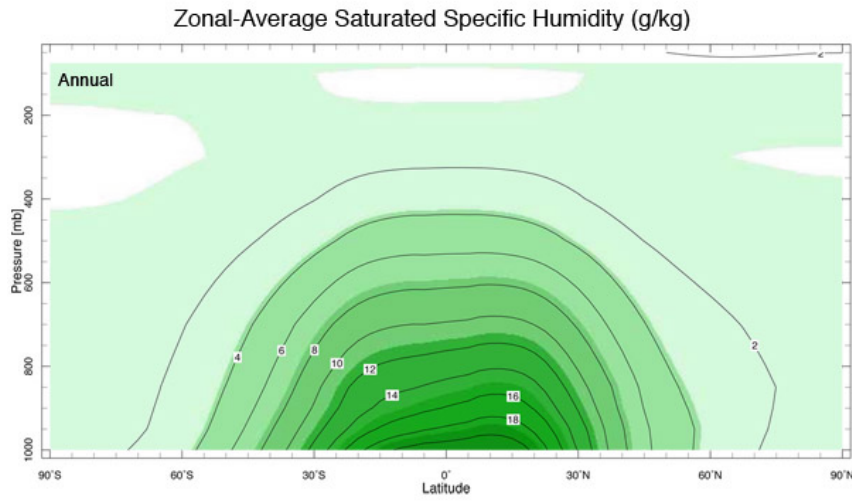


Figure 5.16: Zonally-averaged saturated specific humidity,  $q_*$ , in  $\text{g kg}^{-1}$ , for annual-mean conditions.

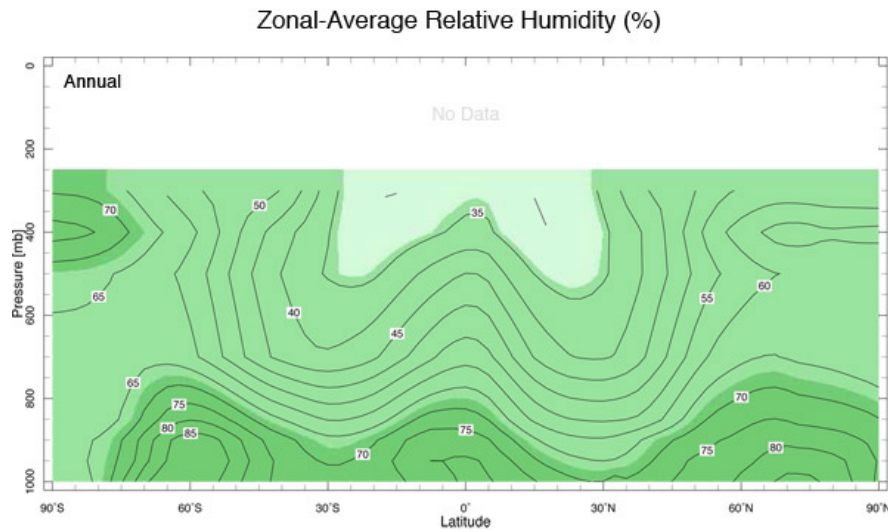


Figure 5.17: Zonal mean relative humidity (%), Eq.(4.25), under annual mean conditions. Note that data is not plotted above 300mb where  $q$  is so small that it is difficult to measure accurately by routine measurements.

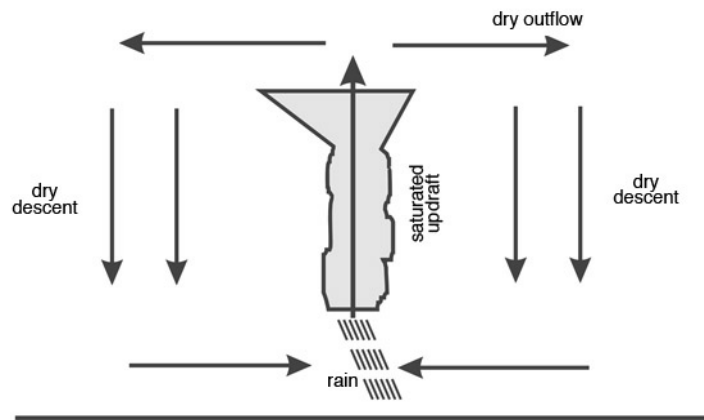


Figure 5.18: Drying due to convection. Within the updraft, air becomes saturated and excess water is rained out. The descending air is very dry. Because the region of ascent is rather narrow and the descent broad, convection acts as a drying agent for the atmosphere as a whole.

of the deserts. (These issues will be discussed further in Chapter 8.)

## 5.4 Winds

We saw in Section 5.2 that because of the pole-equator temperature gradient, isobaric surfaces slope down from equator to pole inducing a horizontal pressure gradient at upper levels. There is thus a pressure gradient force aloft directed from high pressure to low pressure i.e. from warm latitudes to cold latitudes as seen in Fig.5.1. We might expect air to move down this pressure gradient. Hadley<sup>5</sup> suggested one giant meridional cell with rising motion in the tropics and descending motion at the pole, as sketched schematically in Fig.5.19. One might expect rings of air circling the globe to be driven polewards by pressure gradient forces. As they contract conserving the angular momentum imparted to them by the spinning Earth, westerly (W→E) winds will be induced (see detailed discussion in Section 8.2.1). At the poles Hadley imagined that the rings would sink and then expand outward as they flow equatorward below, generating easterly winds, as marked on the figure.

As attractive as this simple circulation may seem, we shall see that this picture of a single meridional cell extending from equator to pole is not in accord with observations.

### 5.4.1 Distribution of winds

Wind velocity is, of course, a vector with components  $\mathbf{u} = (u, v, w)$  in the (eastward, northward, upward) directions. The vertical component is, except in the most violent disturbances, very much smaller than the horizontal components (a consequence, amongst other things, of the thinness of the atmosphere), so much so that it cannot usually be directly measured, but must be inferred from other measurements.

---

<sup>5</sup>George Hadley (1685-1768). British meteorologist who was the first to recognise the relationship between the rotation of the earth and the atmospheric circulation (in particular, the trade winds). Hadley presented his theory in 1735. The pattern of meridional circulation in tropical zones, called the Hadley circulation (or a Hadley cell — see Fig.5.19) is named after him.

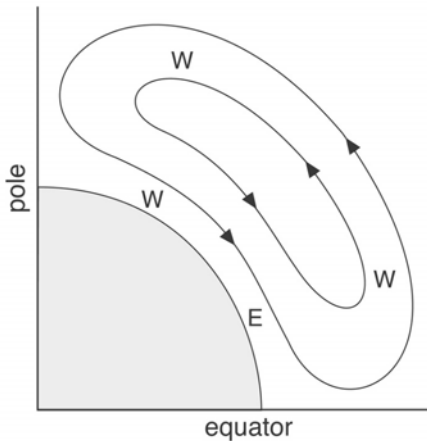


Figure 5.19: The circulation envisaged by Hadley (1735) comprising one giant meridional cell stretching from equator to pole. Regions where Hadley hypothesized westerly (W) and easterly (E) winds are marked.

### Mean zonal winds

The typical distribution of zonal mean zonal wind,  $\bar{u}$ , in the annual mean and at the solstices (December, January, February [DJF] and June, July, August [JJA]) is shown in Fig.5.20. Except close to the equator, the zonal mean winds are eastward (*i.e.*, in meteorological parlance, westerly) almost everywhere. The stronger winds are found at the core of the *subtropical jets*, the strongest of which is located near  $30^\circ$  latitude in the winter hemisphere at 200 mbar at a height of about 10 km with, on average, a speed<sup>6</sup> of around  $30 \text{ m s}^{-1}$ . A weaker jet of about  $20 \text{ m s}^{-1}$  is located near  $45^\circ$  in the summer hemisphere. The easterlies observed in the tropics are much weaker, especially in northern winter.

Note that the winds are much weaker near the ground, but show the same pattern: westerlies poleward of about  $30^\circ$  and easterlies equatorward thereof. The low-level easterlies (which, as we shall see, are actually north-easterlies in the northern hemisphere and south-easterlies in the southern hemisphere) are known as the “trade winds,” a term that comes from the days of sailing ships

---

<sup>6</sup>As we shall see, the jet actually wiggles around, both in longitude and in time, and so is smoothed out in the averaging process. Typical local, instantaneous maximum speeds are closer to  $50 \text{ m s}^{-1}$ .

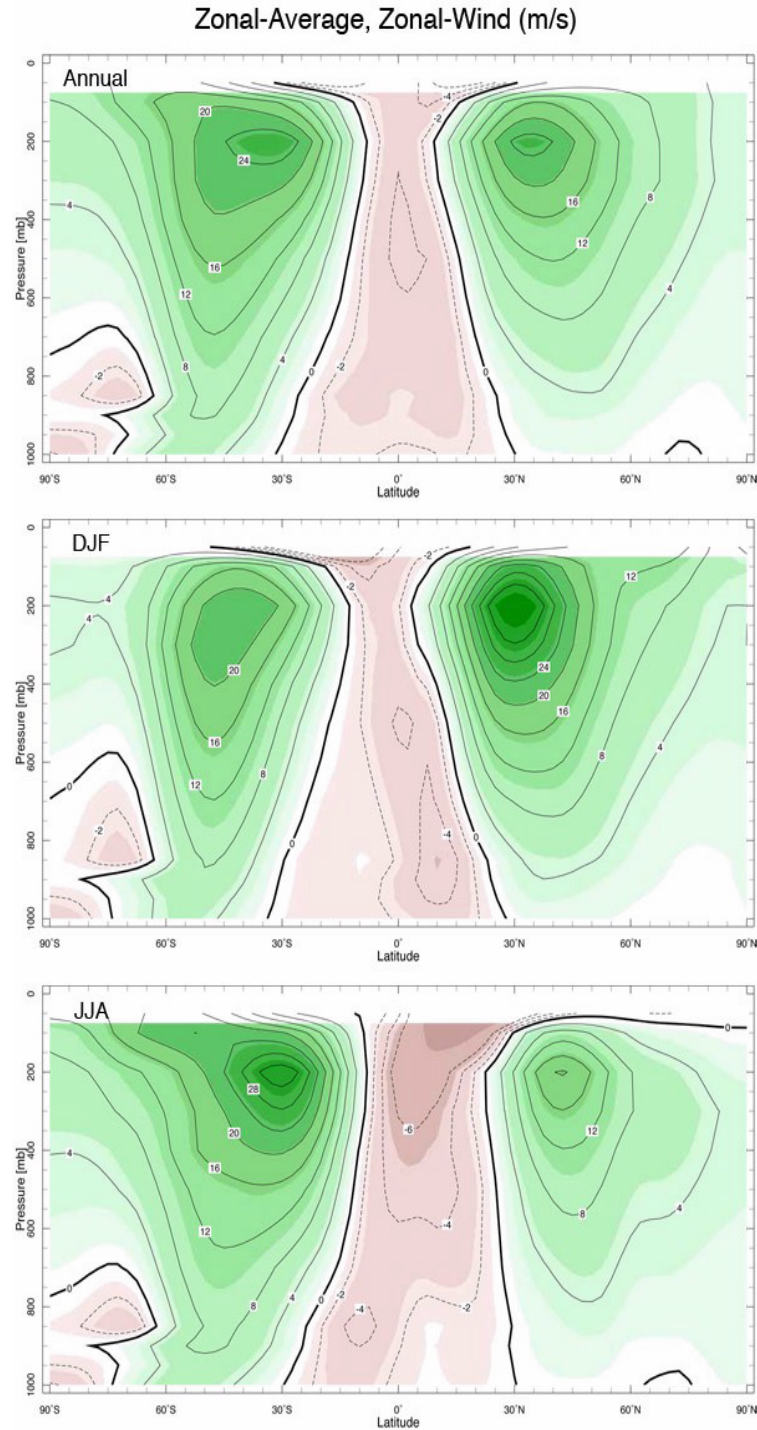


Figure 5.20: Meridional cross-section of zonal-average zonal wind ( $\text{m s}^{-1}$ ) under annual mean conditions (top), DJF (December, January, February) (middle) and JJA (June, July, August) (bottom) conditions.

when, together with the westerlies and south-westerlies of higher latitudes, these winds allowed ships to complete a circuit of the North Atlantic and thus to trade easily between Europe and North America<sup>7</sup>. We shall see later, in Chapter 10, that this pattern of surface winds and the attendant stress is a primary driver of ocean circulation.

### Mean meridional circulation

Fig.5.21 shows the zonal-mean circulation of the atmosphere in the meridional plane — the meridional overturning circulation in height and latitude, whose sense is marked by the arrows. Note the strong seasonal dependence. In DJF air rises just south of the equator and sinks in the subtropics of the northern hemisphere, around 30°N. (Conversely, in JJA air rises just north of the equator and sinks in the subtropics of the southern hemisphere.) We thus see strong upward motion on the summer side of the equator, where the warm surface triggers convection and rising motion, and strong descent on the winter side of the equator. In the annual mean we thus see two (weaker) cells, more or less symmetrically arranged about the equator, one branching north and the other south. Not surprisingly, the regions of mean upward motion coincide with the wet regions of the tropics, as evident, for example, in the presence of cold cloud tops in the OLR distribution shown in Fig.4.26. In contrast, descending regions are very dry and cloud-free. The latter region is the desert belt and is also where the trade inversion discussed in the context of Fig.4.16b is found.

This vertical motion is accompanied by meridional flow. Except in the tropics, mean northward winds are weak ( $< 1 \text{ m s}^{-1}$ ) everywhere. In the tropical upper troposphere (near 200 mbar, between about 20°N and 20°S)



<sup>7</sup> Matthew Fountaine Maury (1806-1873) U.S. Naval officer and oceanographer, the founder of the U.S. Naval Observatory, inventor of a torpedo and pioneer of wind and current charts. Maury was the first to systematically study and map ocean currents and marine winds and recommend routes for sea clippers to take advantage of winds and currents.

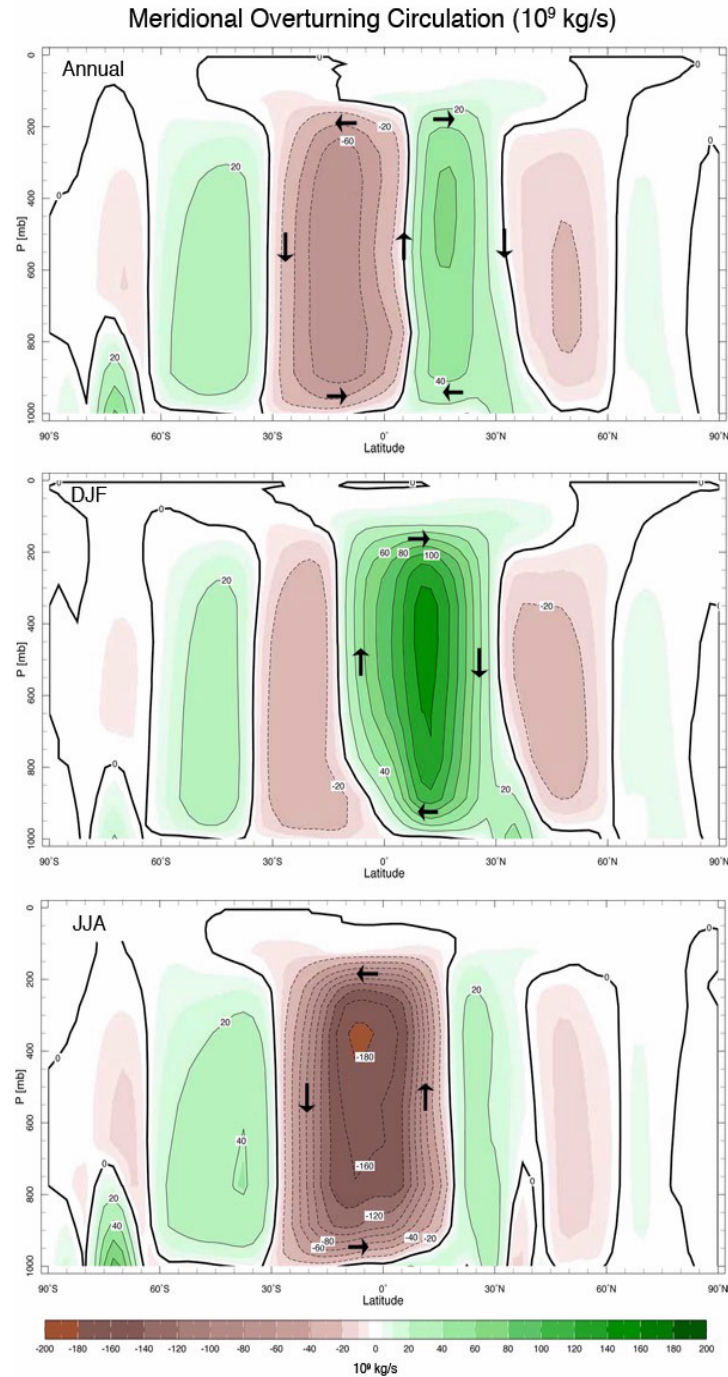


Figure 5.21: The meridional overturning streamfunction  $\chi$  of the atmosphere in annual mean, DJF and JJA conditions. [The meridional velocities is related to  $\chi$  by  $v = -(\rho a \cos \phi)^{-1} \partial \chi / \partial z$ ;  $w = (\rho a^2 \cos \phi)^{-1} \partial \chi / \partial \varphi$ .] Units are in  $10^9 \text{ kg s}^{-1}$ , or Sverdrups as discussed in Section 11.5.2. Flow circulates around positive (negative) centers in a clockwise (anti-clockwise) sense. Thus, in the annual mean, air rises just north of the equator and sinks around  $\pm 30^\circ$ .

we observe winds directed toward the winter hemisphere at speeds of up to  $3 \text{ m s}^{-1}$ . There is a return flow in the lower troposphere that is somewhat weaker, and which is directed mostly toward the summer hemisphere. Thus the “easterlies” we deduced from Fig.5.20 are in fact north-easterlies, north of the equator in northern winter, and south-easterlies, south of the equator in southern winter. These are the *trade winds* mentioned earlier.

The overturning circulation of the tropical atmosphere evident in Fig.5.21 is known as the ‘Hadley cell’; we will consider its dynamics in Chapter 8. The (much) weaker reverse cells in middle latitudes of each hemisphere are known as Ferrel cells, after William Ferrel (1817 - 1891), an American meteorologist who developed early theories of the atmospheric circulation.

### Eddies and waves

Finally, in case the typical, zonally-averaged, cross-sections presented here give the impression that the atmosphere actually looks like this at any given time, note that, in reality, the atmospheric structure is variable in time and three-dimensional. This is evident on any weather map (and from the fact that we need weather forecasts at all). A typical instantaneous 500 mbar geopotential height analysis is shown in Fig.5.22 and should be compared to the (much smoother) monthly average shown in Fig.5.12. Although the general features of the meridional structure are evident (in particular, the decrease of height of the pressure surface from low to high latitude) there are also many localized highs and lows in the instantaneous structure which, as we shall see, are indicative of the presence of *eddies* in the flow<sup>8</sup>. The atmosphere, especially in the extratropics, is full of eddying winds. As will be discussed in Chapter 8, the eddies are the key agency of meridional heat




---

<sup>8</sup> Vilhelm Bjerknes (1862-1951), Norwegian meteorologist. His father, Carl, was a professor of hydrodynamics, while his son, Jacob became a famous meteorologist in his own right (see Chapter 12). With Jacob, he created an early network of meteorological observations. Bjerknes was the founder of the "Bergen school", where the now-familiar synoptic concepts of cyclones, fronts, and air masses were first established.

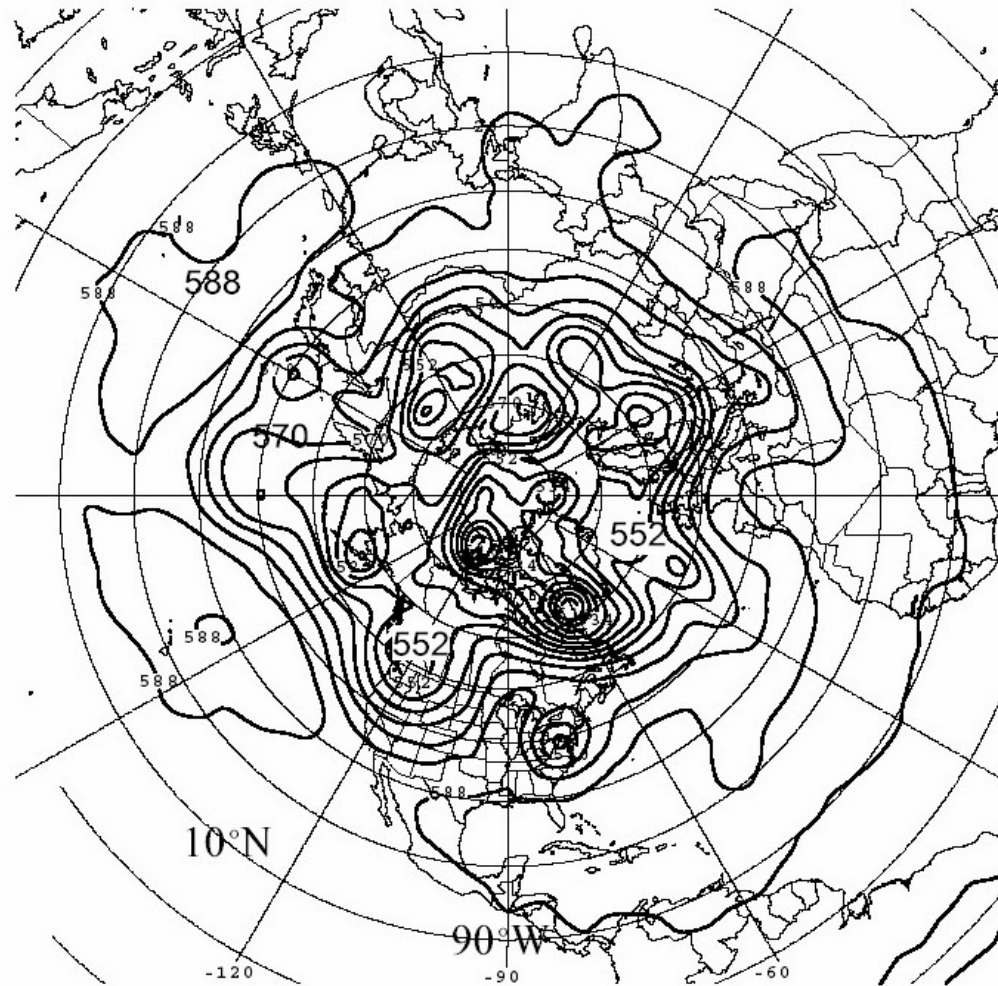


Figure 5.22: Typical 500 mbar height analysis: the height of the 500 mbar surface (in decameters) at 12 GMT on June 21st, 2003. The contour interval is 6 decametres = 60 m. The minimum height is 516 decametres, and occurs in the intense lows over the pole.

and moisture transport in the middle to high latitudes.

In summary, in this Chapter we have discussed how warming of the tropical atmosphere and cooling over the poles leads, through hydrostatic balance, to a large-scale slope of the pressure surfaces and hence pressure gradient forces directed from equator to pole. It turns out that, as we go on to discuss in detail in Chapters 7 and 8, this pressure gradient force is balanced on the large-scale by Coriolis forces acting on the winds due to the earth's rotation. In fact the temperature, pressure and wind fields shown in this chapter are not independent of one another but are intimately connected through basic laws of physics. In order to take our discussion further and make it quantitative, we must next develop some of the underlying theory of atmospheric dynamics. This is interesting in itself because it involves applying the laws of mechanics and thermodynamics to a fluid on a rotating earth, thinking about the importance, or otherwise, of rotation on the fluid motion and contemplating the motion from different frames of reference, that of the rotating earth itself and that of an inertial observer out in space looking back on the earth.

## 5.5 Further reading

A comprehensive survey of the observed climatological state of the atmosphere is given in Chapter 7 of Peixoto and Oort (1992).

## 5.6 Problems

1. Fig.5.5 shows the net incoming solar and outgoing longwave irradiance at the top of the atmosphere. Note that there is a net gain of radiation in low latitudes and a net loss in high latitudes. By inspection of the figure, estimate the magnitude of the poleward energy flux that must be carried by the atmosphere-ocean system across the  $30^\circ$  latitude circle, to achieve a steady state.
2. Suppose that the Earth's rotation axis were normal to the Earth-Sun line. The solar flux, measured per unit area in a plane normal to the Earth-Sun line, is  $S_0$ . By considering the solar flux incident on a latitude belt bounded by latitudes  $(\varphi, \varphi + d\varphi)$ , show that  $F$ , the 24hr-averaged solar flux *per unit area of the Earth's surface*, varies with

latitude as

$$F = \frac{S_0}{\pi} \cos \varphi .$$

- (a) Using this result, suppose that the atmosphere is completely transparent to solar radiation, but opaque to infrared radiation such that, *separately at each latitude*, the radiation budget can be represented by the “single slab” model shown in Fig.2.7. Determine how surface temperature varies with latitude.
  - (b) Calculate the surface temperature at the equator,  $30^\circ$ , and  $60^\circ$  latitude if Earth albedo is 30% and  $S_0 = 1367 \text{ W m}^{-2}$ . Compare your result with observations shown in Fig.5.7.
3. Use the hydrostatic relation and the equation of state of an ideal gas to show that the  $1000 - 500 \text{ mbar}$  “thickness”,  $\Delta z = z(500 \text{ mbar}) - z(1000 \text{ mbar})$  is related to the mean temperature  $\langle T \rangle$  of the  $1000 - 500 \text{ mbar}$  layer by

$$\Delta z = \frac{R \langle T \rangle}{g} \ln 2 ,$$

where

$$\langle T \rangle = \frac{\int T d \ln p}{\int d \ln p} ,$$

where the integrals are from  $500 \text{ mbar}$  to  $1000 \text{ mbar}$ . (Note that  $1000 \text{ mbar} \equiv 1000 \text{ hPa} \equiv 10^5 \text{ Pa}$ ).

- (a) Compute the thickness of the surface to  $500 \text{ mbar}$  layer at  $30^\circ$  and  $60^\circ$  latitude assuming that the surface temperatures computed in Q2b. above extend uniformly up to  $500 \text{ mbar}$ .
- (b) Figs.7.4 and 7.25 (of Chapter 7) show  $500 \text{ mbar}$  and surface pressure analyses for 12GMT on June 21, 2003. Calculate  $\langle T \rangle$  for the  $1000 \text{ mbar}$  to  $500 \text{ mbar}$  layer at the center of the  $500 \text{ mbar}$  trough at  $50^\circ \text{N}, 120^\circ \text{W}$  and at the center of the ridge at  $40^\circ \text{N}, 90^\circ \text{W}$ . [N.B. You will need to convert from surface pressure,  $p_s$ , to height of the  $1000 \text{ hPa}$  surface,  $z_{1000}$ ; to do so use the (approximate) formula

$$z_{1000} \cong 10 (p_s - 1000) ,$$

where  $z_{1000}$  is in meters and  $p_s$  is in hPa.]

Is  $\langle T \rangle$  greater in the ridge or the trough? Comment on and physically interpret your result.

4. Use the expression for saturated specific humidity, Eq.(4.24) and the empirical relation for saturated vapor pressure  $e_s(T)$ , Eq.(1.4) (where  $A = 6.11 \text{ mbar}$  and  $\beta = 0.067 \text{ }^{\circ}\text{C}^{-1}$  and  $T$  is in  $^{\circ}\text{C}$ ) to compute from the graph of  $T(p)$  in the tropical belt shown in Fig.4.9, vertical profiles of saturated specific humidity,  $q^*(p)$ . You will need to look up values of  $R$  and  $R_v$  from Chapter 1.

Compare your  $q^*$  profiles with observed profiles of  $q$  in the tropics shown in Fig.5.15. Comment?

